Impedance Optimization for Uncertain Contact Interactions Through Risk Sensitive Optimal Control

Bilal Hammoud^{1,2}, Majid Khadiv² and Ludovic Righetti^{1,2}

Abstract—This paper addresses the problem of computing optimal impedance schedules for legged locomotion tasks involving complex contact interactions. We formulate the problem of impedance regulation as a trade-off between disturbance rejection and measurement uncertainty. We extend a stochastic optimal control algorithm known as Risk Sensitive Control to take into account measurement uncertainty and propose a formal way to include such uncertainty for unknown contact locations. The approach can efficiently generate optimal state and control trajectories along with local feedback control gains, i.e. impedance schedules. Extensive simulations demonstrate the capabilities of the approach in generating meaningful stiffness and damping modulation patterns before and after contact interaction. For example, contact forces are reduced during early contacts, damping increases to anticipate a high impact event and tracking is automatically traded-off for increased stability. In particular, we show a significant improvement in performance during jumping and trotting tasks with a simulated quadruped

Index Terms—Humanoid and Bipedal Locomotion, Legged Robots, Motion Control, Optimization and Optimal Control.

I. INTRODUCTION

S TATE of the art locomotion controllers include a model predictive control scheme that computes trajectories of some reduced model. This model predictive scheme is then realized through a pre-designed impedance controller or a QP based inverse dynamics solver. These strategies have proven to be successful in completely structured and controlled environments. However, current robot control strategies still lack the ability to reason about uncertainty in the environment. High stiffness feedback controllers are usually used to track precise trajectories. This approach is usually limiting for a robot in multi-contact scenarios where the robot depends on intermittent contact interactions to move itself or some object around. Contact interactions increase the complexity of the control design problem. A stiff controller will counteract an unpredicted contact by increasing the control input to ensure tracking, which might generate high contact forces that destabilize the system. On the other hand, excessive compliance

Manuscript received: October, 15, 2020; Revised January, 18, 2021; Accepted February, 25, 2021.

This paper was recommended for publication by Editor A. Kheddar upon evaluation of the Associate Editor and Reviewers' comments. This work was supported by New York University, the European Union's Horizon 2020 research and innovation program (grant agreement 780684 and European Research Council's grant 637935) and the National Science Foundation (grants 1825993, 1932187, 1925079 and 2026479).

¹Tandon School of Engineering, New York University, USA bah436,1r114@nyu.edu

²Max Planck Institute for Intelligent Systems, Tübingen, Germany first.last@tuebingen.mpg.de

Digital Object Identifier (DOI): see top of this page.

could lead to large deviations from the desired task. Studies from the field of neuroscience suggest that human beings modulate their impedance during contact interactions [1], [2]. Other studies suggest that sensorimotor commands are the result of an optimal feedback control mechanism that controls a trade-off between accuracy and stability [3]. A more recent study [4] suggests that this impedance "sweet spot" is a result of reasoning not only about the desired task, but also the uncertainties present during contact interactions.

Impedance control for robotics was postulated and derived by Hogan [5]. Hogan [6] also demonstrated experimentally that this controller is capable of stabilizing contact interactions if proper impedance parameters were to be chosen. Following the results presented by Hogan, Park [7] used a similar approach to design a bipedal walking controller. The results show a biped capable of walking on uneven terrain. The results achieved through impedance control have proven to be superior for control strategies involving contact interactions [8]. However, the mentioned approaches design the impedance schedules through an exhaustive trial and error process. It remains an open question on how to systematically optimize impedance profiles for robotic tasks involving contact interactions.

Optimal feedback control theory has many promising aspects that could help approach this problem. Mayne [9] introduced an algorithm that computes local quadratic approximations of both the dynamics and the cost functions and then iteratively solves the nonlinear optimal control problem. This algorithm is commonly known as the Differential Dynamic Programming Algorithm (*DDP*). It has the advantage of providing an optimal control trajectory together with local feedback controller. Many variations of *DDP* appeared later in the literature [10], [11], [12], [13], [14], [15]. However, all the mentioned variations are deterministic in nature and favor tracking over stability, making them prone to failure in situations where tracking cannot be perfectly achieved, and in attempting to do so, the controller can destabilize the system, uncertain contact interactions being a clear example.

Todorov [16] added multiplicative process noise to the optimal control problem violating the certainty equivalence principle. This led to control policies that are dependent on the process noise. Li [17] derived similar results for partially observable systems with control constraints resulting in control policies that are a function of both process and measurement uncertainties. Another method to break the certainty equivalence principle is achieved through an exponential transformation of the cost function, this was first introduced by Jacobson [18] for linear systems and later extended for nonlinear optimal control by Farshidian [19]. This formally

synthesizes a controller that could obtain risk neutral, risk sensitive or risk seeking behaviors depending on the parameterization of the role of the uncertainty in the cost function. Medina [20] used the exponential cost transformation with process noise to perform manipulation tasks through a model predictive control scheme. The exponential transformation was extended to accommodate for measurement uncertainties in [21] obtaining a risk sensitive optimal control algorithm that accounts for higher order statistics in both process and measurement models making it a suitable framework for designing feedback controllers that can trade-off disturbance rejection and measurement uncertainty. The approach was only tested on toy problems and never used for more complex robotic tasks.

This paper builds on the ideas of Ponton [21] to propose a systematic method for computing impedance schedules for legged robots. We extend the algorithm to work with hard contact transitions and introduce a way to incorporate contact measurement uncertainty into the whole-body optimal control formulation. This results in systematically optimized impedance profiles that exhibit desirable stiffness and damping patterns to handle uncertain, high impact and contact transitions. Extensive numerical simulations demonstrate the properties of the approach when compared to usual DDP algorithms and other measurement noise models. In particular, we show a significant increase in performance for hard impacts for jumping and trotting over uneven terrains.

II. BACKGROUND

This section provides background on the robot and contact models, risk-sensitive stochastic optimal control and its extension to include measurement uncertainty.

A. Multi-Contact Robot Dynamics

The dynamics of a legged robot in contact with its environment is described using the following equation

$$\underbrace{\frac{d}{dt} \begin{bmatrix} q \\ v \end{bmatrix}}_{\hat{x}} = \underbrace{\begin{bmatrix} v \\ M^{-1}(\tau - h + J^T \lambda_{ext}) \end{bmatrix}}_{f(x,y)} \tag{1}$$

where $q = \begin{bmatrix} x,y,z,q_1^B,\dots,q_4^B,\theta_1,\dots,\theta_{nj} \end{bmatrix}^T \in SE(3) \times R^{nj}$ includes the base cartesian position x,y,z, the base orientation parametrized as quaternions q_i^B and θ_j being j-th joint of the robot. $v \in R^{nv}$ is the vector of generalized velocities with nv = nj + 6 and expressed in the base local frame. M(q) is the inertial matrix, h(q,v) is the vector combining the nonlinear terms such as Coriolis acceleration and gravity, S^T is the selection matrix mapping the controls to the actuated degrees of freedom, λ_{ext} is the vector of contact forces and J(q) is the contact Jacobian. The notation indicating the dependence on q and v will be omitted for the remainder of the text. Let $x^T = \begin{bmatrix} q^T, v^T \end{bmatrix}$ define the state vector, hence the discrete time state transitions become

$$x_{t+1} = f_t(x_t, u_t) = x_t \oplus \underbrace{(\delta t f(x, u))}_{dx_t}$$
 (2)

Then dx_t represents the change in the state vector during a time interval δt and \oplus handles the Lie group composition operation for the base orientation.

B. Rigid Contact Model

While different contact models can be chosen to compute the contact forces λ_{ext} [22], a rigid contact model is chosen for the optimal control computation [23]. Let p, \dot{p} and \ddot{p} denote any contact point position, velocity and acceleration respectively, then during an active contact phase, the rigid contact assumption can be stated as

$$\dot{p} = Jv = 0 \quad \text{and} \quad \ddot{p} = \dot{J}v + J\dot{v} = 0. \tag{3}$$

In order to resolve the contact forces that guarantee the no-motion constraints of all active contacts, the robot dynamics (1) is projected to the contact space using $\left(JM^{-1}J^{T}\right)^{-1}JM^{-1}=\Lambda JM^{-1}$ to result in

$$\lambda_{ext} = -\Lambda \dot{J}v + \Lambda J M^{-1} h - \Lambda J M^{-1} S^T \tau \tag{4}$$

Once λ_{ext} is obtained, the motion vector dx_t can be computed and the state vector x_{t+1} can be obtained from (2).

C. Risk Sensitive Optimal Control

We consider the stochastic optimal control approach known as Risk Sensitive Control to explicitly reason about uncertainty. A nonlinear iterative risk sensitive optimal control formulation [24], [19], [21] explicitly takes into account the distribution of uncertainty while being numerically efficient for nonlinear problems. Consider the following dynamics written as a nonlinear stochastic difference equation

$$x_{t+1} = f_t(x_t, u_t) + F(x_t, u_t) \omega_t$$
 (5)

where $\omega_t \sim \mathcal{N}\left(0, \Omega_t\right)$ is the process noise which accounts for unmodeled disturbances and $F(x_t, u_t)$ maps the noise to the full state. Consider an objective function of the form

$$\mathcal{L}(\mathcal{X}, \mathcal{U}) = l_T(x_T) + \sum_{t=0}^{T-1} l_t(x_t, u_t)$$
 (6)

where $\mathcal{X} = [x_0,...,x_T]$ and $\mathcal{U} = [u_0,...,u_{T-1}]$ denote the state and control trajectories respectively, $l_T(x_T)$ is the terminal cost, and $l_t(x_t,u_t)$ is the cost at time t. Typical optimal control approaches minimize the expectation of the objective function, however, risk sensitive optimal control instead minimizes the expectation of the exponential transformation of the objective. This affords the consideration of the higher-order statistics of the cost

$$\mathcal{J}^* = \min_{\mathcal{X},\mathcal{U}} \mathbb{E} \left[\exp \left(\sigma \mathcal{L} \left(\mathcal{X}, \mathcal{U} \right) \right) \right] \tag{7}$$

where σ is the sensitivity scalar. Farshidian [19] proved that the cumulant generating function of \mathcal{J} can be expressed as

$$\frac{1}{\sigma}\log \mathcal{J} = \mathbb{E}\left[\mathcal{L}\right] + \frac{\sigma}{2}\mu_2\left[\mathcal{L}\right] + \frac{\sigma^2}{6}\mu_3\left[\mathcal{L}\right] + \dots \tag{8}$$

where $\mu_i[\mathcal{L}]$ is the *i*'th moment of the random variable \mathcal{L} . The risk sensitivity parameter σ then provides a tool to control the contribution of the higher order moments on the cost. When $\sigma < 0$, the control is risk-seeking and higher cost variances will be preferred. When $\sigma > 0$, the control is risk-averse since a high variance of the cost distribution will be more penalized. When $\sigma \to 0$, the problem reduces to a normal

(risk-neutral) optimal control problem and only the expectation of the objective is minimized.

The problem can be solved globally with Riccati-like equations for linear dynamics and a quadratic objective function [18], the solution being a linear feedback controller. However, finding a global minimizer $\mathcal{X}^*, \mathcal{U}^*$ for the cost function (7) is generally intractable for nonlinear dynamics and non quadratic costs. The method presented in this paper computes locally optimal solutions through iterative linearizations of the dynamics and a quadratic approximation of the objective functions, a common technique used in deriving iterative nonlinear optimal control algorithms [9], [13], [19], [25]. The local deviations from nominal state and control trajectories, denoted by superscript n, are written as

$$\delta x_t = x_t \ominus x_t^n, \qquad \delta u_t = u_t - u_t^n \tag{9}$$

with \ominus representing the suitable difference on the state manifold. The system dynamics can be linearized in terms of the deviations as

$$\delta x_{t+1} = A_t \delta x_t + B_t \delta u_t + C_t \omega_t \tag{10}$$

where A_t , B_t and C_t are the respective linearization of $f_t(\delta x_t, \delta u_t)$ and $F_t(\delta x_t, \delta u_t)$ with respect to the state and control terms. Similarly a quadratic approximation of the cost function $l_t(x_t, u_t)$ can be obtained. For a linear dynamics and a quadratic cost under the risk sensitive exponential transformation, the value function takes the form of an exponential with a quadratic argument in the state [18]

$$V\left(\delta x_{t}\right) = \exp\left\{\sigma\left(\frac{1}{2}\delta x_{t}^{T} S_{t} \delta x_{t} + \delta x_{t}^{T} s_{t} + \bar{s}_{t}\right)\right\}$$
(11)

Importantly, the value function here holds a completely different form than that of DDP and the principle of optimality needs to be written in multiplicative form as

$$V\left(\delta x_{t}\right) = \min_{\delta u_{t}} \left\{ \exp\left[\sigma l_{t}\left(\delta x_{t}, \delta u_{t}\right)\right] \mathbb{E}\left[V\left(\delta x_{t+1}\right)\right] \right\}$$
 (12)

In order to obtain the solution, the expectation of the value function at time t+1 must be computed. Finally the value function at time t is approximated by computing S_t, s_t and \bar{s}_t along with δu_t recursively backward in time. Since δu_t is the argument minimizing a quadratic in δx_t , then the locally optimal controller $\delta u_t = K_t \delta x_t + k_t$ is linear in the state deviations. Here, K_t is the error feedback gains while k_t is the feedforward command. The solution of the recursive risk sensitive value function is discussed in details in [18], [19]. The optimized deviations are used to iteratively improve the solution until convergence is reached. It is important to note that the control law explicitly incorporates the covariance of the noise distribution in K_t and k_t [19].

D. Including Measurement Uncertainty

The formulation presented above does not integrate the uncertainty coming from a nonlinear measurement model

$$y_{t+1} = q(x_t, u_t) + H(x_t, u_t) \gamma_t$$
 (13)

where $\gamma_t \sim \mathcal{N}\left(0, \Gamma_t\right)$ is the measurement noise. Measurement uncertainty is crucial for our approach as we need

to take into account the uncertainty about contact locations. Speyer [26] incorporated measurement noise into the risk sensitive formulation by introducing a state vector that grows at each time step to include the entire history of the states. Recently, Ponton [21] suggested that this could be avoided by augmenting the linearized system dynamics with that of an Extended Kalman Filter (EKF). Assuming an observable system, an EKF can be used to compute the estimate deviations $\delta \hat{x}_t$ along the nominal trajectory at each iteration. Let F_t and D_t be the linear approximations of $g(x_t, u_t)$ and $H(x_t, u_t)$ from (13) respectively. Then we can compute the Kalman gains G_t during the forward pass of the iterative algorithm (i.e. when updating the nominal state and control trajectories) and use them to define an augmented linear system, which includes both the real, δx_t , and estimated, $\delta \hat{x}_t$, states of the system. With the extended state $\delta \tilde{x}_t = [\delta x_t, \delta \hat{x}_t]$, the augmented system dynamics becomes

3

$$\begin{bmatrix} \delta x_{t+1} \\ \delta \hat{x}_{t+1} \end{bmatrix} = \begin{bmatrix} A_t \delta x_t + B_t \delta u_t \\ A_t \delta x_t + B_t \delta u_t + G_t F_t (\delta x_t - \delta \hat{x}_t) \end{bmatrix} + \begin{bmatrix} C_t & 0 \\ 0 & G_t D_t \end{bmatrix} \begin{bmatrix} \omega_t \\ \gamma_t \end{bmatrix}$$
(14)

This augmented linear dynamical system is used, in place of (10), to solve the risk sensitive problem. The resulting locally optimal control policy is then

$$\delta u_t^* = k_t + \begin{bmatrix} K_t^x & K_t^{\hat{x}} \end{bmatrix} \delta \tilde{x}_t \tag{15}$$

As the true state deviations δx_t are unknown, then following Li [17] and Ponton [21], we take the expectation of δu_t^* with δx_t conditioned on $\delta \hat{x}_t$ to give the optimal policy

$$\mathbb{E}_{\delta x_t | \delta \hat{x}_t} \left[\delta u_t^* \right] = k_t + \left(K_t^x + K_t^{\hat{x}} \right) \delta \hat{x}_t \tag{16}$$

Detailed derivations of the complete recursive algorithm follow the work of Ponton [21] and can be found together with our software implementation in our open-source repository¹. It is also important to note that the backward recursion has the same complexity as that of DDP. The only added complexity is the computation of the estimator gains in the forward pass. The convergence of iterative risk sensitive solvers is studied in the work of Roulet [27].

III. MULTI-CONTACT RISK SENSITIVE CONTROL

Now we detail how we use the risk-sensitive optimal control algorithm including measurement uncertainties to optimize motions and impedance schedules for legged robots.

A. Including Multiple Contact Switching

For the rigid contact model (3), a contact switch causes a change in the dimensions of the contact Jacobian J. Given a predefined contact sequence and timing we can define the switching in the overall system dynamics denoted f_n where the subscript n indicates a predefined contact phase. The contact switching sequence is obtained with an initial guess for the open-loop optimal trajectory using an existing kino-dynamic optimizer [28]. The contact transitions are also aligned with

¹https://github.com/machines-in-motion/risk_sensitive_control

the collocation points such that the objective function and dynamics of the problem can be written as

$$\min_{\delta X, \delta U} \mathbb{E} \left[\exp \left(\sigma l_T \left(\delta x_T \right) + \sigma \sum_{n=0}^{N} \sum_{t=0}^{T} l_t \left(\delta x_t, \delta u_t \right) \right) \right]$$

$$s.t. \quad \delta x_{t+1} = f_n \left(\delta x_t, \delta u_t \right)$$
(18)

where $\delta\mathcal{X}$ and $\delta\mathcal{U}$ are the trajectories of the state and control deviations respectively. N is the number of contact switches along the trajectory, and T is the horizon of each phase. This procedure avoids non-smooth switches in the contacts by solving the optimal control problem on multiple smooth intervals. Consistency at the transition between the switching intervals is ensured through the forward integration of the trajectory along with high penalty on tracking the switching states. In particular, we compute analytical derivatives for all the quantities, including the contacts, using the Pinocchio and Crocoddyl libraries [29], [25].

B. Error State Kalman Filter on Smooth Manifolds

It is desired to design an EKF to augment the linearized dynamics of the robot at each time step, hence, the same dynamical model f_n is used, i.e. at each time step, the predefined contact sequence defines the dynamical model of choice. Let the discrete time EKF of the state deviations $\delta \hat{x}_t$ take the form of the second row of (14), then following [21] the error dynamics $\delta e_{t+1} = \delta x_{t+1} - \delta \hat{x}_{t+1}$ is given by

$$\delta e_{t+1} = (A_t - G_t F_t) \, \delta e_t + C_t \omega_t - G_t D_t \gamma_t \tag{19}$$

This is the simplest estimator of choice and can be replaced with any other estimator as long as it can be written locally as a linear dynamical system. The optimal estimation gains are then given by

$$G_t = A_t \Sigma_t F_t^T \left(F_t \Sigma_t F_t^T + D_t \Gamma_t D_t^T \right)^{-1}$$
 (20)

where Σ_t is the error dynamics covariance. As legged robots have a free floating base modeled as an SE(3) element, the proper Lie group operations must be utilized during the propagation of the covariance of the local error dynamics. A full treatment of EKFs on Lie groups can be found in [30].

C. Uncertainty in Contact Interactions

Consider a robot during a dynamic contact scenario as depicted in Fig. 1. A control algorithm computes actuation torques based on the perception of the robot's own states along with its surrounding environment. Both the perception of the robot environment and its states are susceptible to sensor noise and perception errors, introducing uncertainty in the measurements. We propose to model the contact uncertainty as an uncertainty at the tip of the swing foot Γ_c as shown in the ellipsoid in Fig. 1. This has the advantage of avoiding the need to keep track of the environment model or the next contact location in the state vector. We then map this uncertainty back to the space where the full state covariance matrix Γ_{fs} is defined. Adding both covariances results in the total uncertainty in the contact interaction.



Fig. 1: Uncertainty in Contact Interactions

A deviation in the swinging end-effector of the robot can be linearly mapped to a deviation in its state vector through

$$\begin{bmatrix} \delta p \\ \delta \dot{p} \end{bmatrix} = \underbrace{\begin{bmatrix} J_s & 0 \\ \dot{J}_s & J_s \end{bmatrix}}_{A} \begin{bmatrix} \delta q \\ \delta v \end{bmatrix}$$
 (21)

where J_s is the jacobian of the swinging foot. Then the minimum norm change in the state vector corresponding to a change in the end-effector is given by

$$\begin{bmatrix} \delta q \\ \delta v \end{bmatrix} = A_s^{\dagger} \begin{bmatrix} \delta p \\ \delta \dot{p} \end{bmatrix} \tag{22}$$

where $A_s^\dagger = A_s^T \left(A_s.A_s^T\right)^{-1}$ is the Moore-Penrose inverse of A_s . Different norms could be chosen using a weighted inverse if desired. Now that the deviations of the end-effector are in the same vector space as the full state errors, it is possible to add the noise resulting from the robot states such as joint encoders along with the contact uncertainty. However, a deviation in the swing foot might induce a deviation in the feet that are actively in contact and break our rigid constraint assumption in (3). To avoid inconsistency, the deviations of the swing foot must be projected to the null space of the feet actively in contact using the null space projector P_c . The final form of the deviations transformation can then be written as

$$\begin{bmatrix} \delta q \\ \delta v \end{bmatrix} = \underbrace{\left(I - A_e^{\dagger} A_e\right)}_{P_e} A_s^{\dagger} \begin{bmatrix} \delta p \\ \delta \dot{p} \end{bmatrix} \tag{23}$$

where A_c is similar in structure to A_s however containing the Jacobians of the active contacts described in (3). This transformation maps the mean of the deviations in a certain end-effector frame to that of the full state vector of the robot. Since our noise model is Gaussian, the covariance matrix can also be transformed using the affine property of Gaussians. The total covariance of the state vector becomes

$$\Gamma = \Gamma_{fs} + P_c A_s^{\dagger} \Gamma_c A_s^{\dagger T} P_c^T \tag{24}$$

In summary, we define Gaussian noise models both in endeffector and state space, with respective covariance Γ_c and Γ_{fs} . We combine them using (24). This approach allows to modulate uncertainty at the feet just before and after contact.

IV. SIMULATIONS RESULTS

To demonstrate the capabilities of the proposed method for controlling multi-contact interactions under contact uncertainty, we present three different simulation experiments using an accurate model of our open-source quadruped robot Solo [31]. In the first experiment, we study the effect of different measurement noise models on the computed impedance profiles and resulting impact forces when encountering an unexpected contact. With the second experiment, we explore how the trade-off between stiffness and damping changes

5

when using our risk-sensitive control approach when compared to standard DDP methods. Finally, in the third experiment, we systematically quantify how the stability of the system is favored relative to the accuracy of the controller in the risk sensitive case during locomotion tasks.

The DDP controller used as a baseline in the presented experiments is from [25]. The kino-dynamic optimizer described in [28] is used to generate reference trajectories around which both iterative controllers DDP and Risk Sensitive are initialized. A linear spring damper contact model is used for the simulations with an explicit Euler integration scheme [32] at a time step $\delta t_{sim} = 1e-4s$ with a spring stiffness parameter of $k = 1e5 \,\mathrm{N/m}$ and a spring damping parameter of b =3e2Ns/m. The coefficient of static friction used in simulation is $\mu = 0.7$. The simulated feedback control frequency runs at 1kHz and the discretization step for the optimal control problems is set to $\delta t_{opt} = 1\mathrm{e}{-2}\,\mathrm{s}$. Moreover, the legs of the robot will be referred to as FL, FR, HL, HR denoting FrontLeft, FrontRight, HindLeft and HindRight respectively. Each leg of the robot in turn consists of three joints as it can be seen in Fig. 1.

For all the experiments, the same cost function, weights and reference trajectories are used for both DDP and Risk Sensitive Control. All the planning and control is designed for perfectly flat floor in all three experiments. This results in the same whole body trajectories x_t and the same feedforward torque control profiles τ for both DDP and Risk Sensitive control in each experiment. The sensitivity parameter is set to $\sigma=10$ for the Risk Sensitive solver, leaving the uncertainty models as the only variable in the experiments. The only differences in the optimized plans are the impedance profiles (i.e. the feedback gains K_t).

For all the experiments presented, the uncertainty parameters can be described as follows. The process noise $\Omega_t = diag(1\mathrm{e}{-6})$ through out the whole experiment. The full state measurement noise $\Gamma_{fs} = diag(5\mathrm{e}{-3})$ for all the experiments. $\Gamma_c = 0$ during any lift off phase of the foot. For the landing phase Γ_c is increased to $5\mathrm{e}{-4}$ for the diagonal elements corresponding to p and $1\mathrm{e}{-4}$ for the diagonal elements corresponding to \dot{p} .

A. Effect of Noise Models on Impedance Regulation

In this experiment, the task is to swing a single leg forward with a maximum height of $10\,\mathrm{cm}$ and a step length of $8\,\mathrm{cm}$ similar to what is shown in Fig. 1. A $3\,\mathrm{cm}$ high block is added at the next contact location to simulate an unpredicted contact of 9.2% of the total leg length. The contact with the block occurs at $t=0.43\,\mathrm{s}$ whereas the contact with flat ground was planned for $t=0.55\,\mathrm{s}$.

The first uncertainty model, *Risk-Uniform*, is simply a diagonal matrix with equal variance on all of its entries. In the second uncertainty model, *Risk-SwingJoints*, the variance terms on the joints of the swinging foot are increased. In the third model, *Risk-Unconstrained*, we add a contact noise term similar to (22) without using the nullspace projection due to the active contacts. The last model, *Risk-Contact*, includes the projection of the swing contact uncertainty into the null space of the active contacts (23).

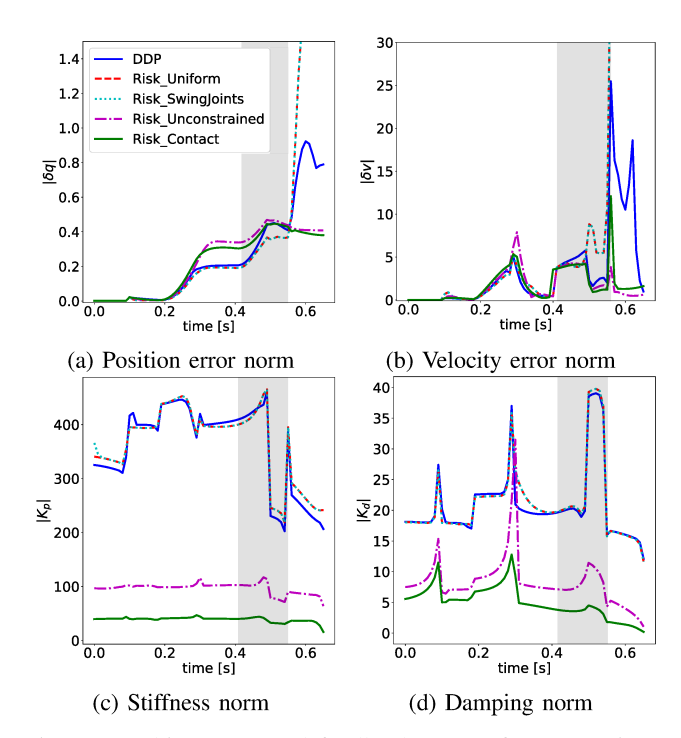


Fig. 2: Tracking error and feedback norms for uncertainty models and DDP. The grey zone corresponds to the time between the unexpected contact and the planned one.

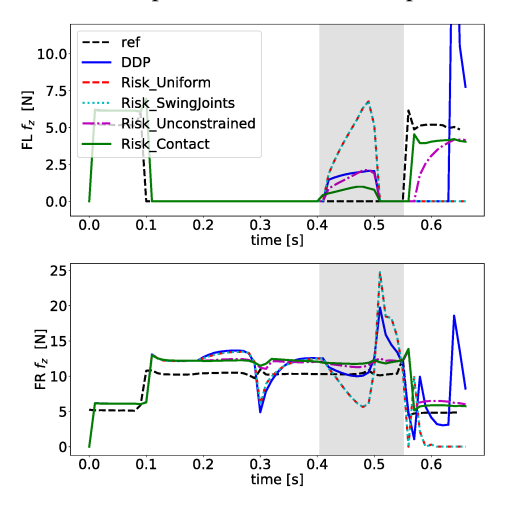


Fig. 3: Front feet normal forces for different uncertainty models and DDP.

Figure 2 compares the tracking behavior of each control scheme. The state error is divided into the error in the configuration δq (Fig. 2a) and the error in the velocity tracking δv (Fig. 2b). Similarly the optimized feedback gains are divided into the feedback gains associated to the configuration K_p and the feedback gains from the velocity K_d . Their norms are shown in Fig. 2c and Fig. 2d respectively. The vector norm $\|v\| = \sqrt{v^T v}$ is used to compute the state error norms whereas the Frobenius Norm $\|M\|_F = \sqrt{Trace\left(MM^T\right)}$ is used to compute the feedback norms.

We notice in Fig. 2 that the risk sensitive control with Risk-Uniform and Risk-SwingJoint noise models diverge after the unexpected impact. DDP also diverges but accumulates less error than these two risk sensitive schemes. All three controllers have high gain norms at the time of impact $|Kp| \approx 400$ and a stiffness to damping ratio at $|Kp|/|Kd| \approx 20$. It is important to note that such gains are too high and would not be usable on the real robot [31]. The maximum reduction in the overall stiffness and damping is obtained by using the Contact uncertainty model where $|Kp_{DDP}|/|Kp_{Contact}| \approx 10$ and $|Kd_{DDP}|/|Kd_{Contact}| \approx 4$. With this reduction in the impedance magnitudes, a less accurate tracking is observed for both Unconstrained and Contact earlier in time $t=0.3\,\mathrm{s}$. However, thanks to the less aggressive feedback gains, the robot can handle the unpredicted impact. Importantly, these reduced gains fit well within ranges acceptable for execution on the real robot.

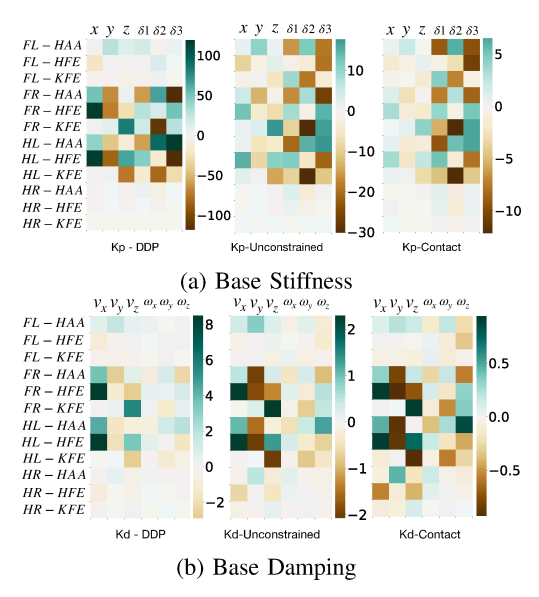


Fig. 4: Part of the feedback gains mapping base errors to joint torques at the time of unexpected impact t = 0.43 s

The effect of the controllers is clearer when looking at the normal contact forces (Fig. 3) where the impact force on the swinging leg FL after $t=0.43\,\mathrm{s}$ is lowest for Risk-Contact. Additionally, the impact force propagates its effect to the front right leg for DDP, Risk-Uniform and Risk-SwingJoints. Whereas for the case where the uncertainty about the contact is included (Risk-Unconstrained and Risk-Contact), we see that the robot absorbs the impact force and we do not notice any propagation of the disturbance to the other feet.

Inspecting the structure of the feedback matrices computed at the time of impact can shed light on these differences in behavior. The blocks of the feedback matrix that map the base states to the control are depicted in Fig. 4. Risk Sensitive control changes the structure of the gain matrices, where the base error is modulated mainly through the feet on the ground namely FR, HL and HR, which is expected. The advantage of Risk-Contact is observed in the portion of the feedback matrix that maps the joint errors to the control commands (Fig. 5). DDP has aggressive Kp gain to track the motion of the swinging foot FL, that is the first three diagonal elements of Kp-DDP relative to the remaining diagonal elements corresponding to the remaining joints. Unlike Kp-DDP and Kp-Unconstrained, Kp-Contact has lower gains on the joints of FL relative to the joints of the support feet FR and HL. This

allows the swing foot to behave as a soft spring relative to the support feet which explains the significantly lower impact force observed and the good tracking of the contact forces on the other feet. These results underline the importance of choosing appropriate noise models and supports the choice of the Risk-Contact noise model.

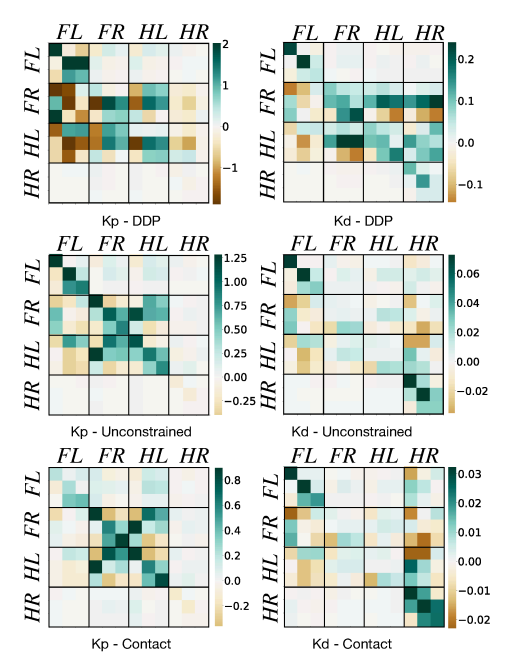


Fig. 5: Part of the feedback gains mapping joint errors to joint torques at time of unexpected impact $t = 0.43 \,\mathrm{s}$

B. Stiffness vs. Damping & Impact Forces

We now only consider the Risk-Contact noise model. This experiment discusses how the introduced model results in an improvement of the performance of an extremely dynamic motion, a jump of a total height of 0.5 m. Halfway through the flight phase, a block of 3 cm height is placed on the floor.

Both *DDP* and Risk-Contact feedback policies achieve the desired jump height with a slightly better performance for the DDP controller. However, inspecting the tracking and impedance profiles reveals a more natural behavior emerging in the Risk Sensitive case. During the flight phase between $t = 1\,\mathrm{s}$ and $t = 1.5\,\mathrm{s}$ both controllers exhibit a significant decrease in both the base and joint stiffness as shown in Fig. 6. For the damping portion of the feedback matrix, the base damping also shows a decrease during the flight phase. Remarkably, we notice a stark difference in the damping modulation of the joints. DDP significantly decreases damping on the joints while Risk Sensitive significantly increases it. This substantial increase in the joint damping allows to more quickly absorb the unexpected impact, i.e. an abrupt change in the velocity of the feet. As a result, we notice 20% lower impact forces (Fig. 8), which in turn avoids the bouncing behavior observed with the DDP controller (Fig. 9). This comes however at the cost of larger deviations for the joint positions. When measuring the stiffness to damping ratio of both the base and the joints, we notice that during active contact phases the base stiffness to damping ratio is relatively the same for DDP and risk sensitive. However, for the joints,

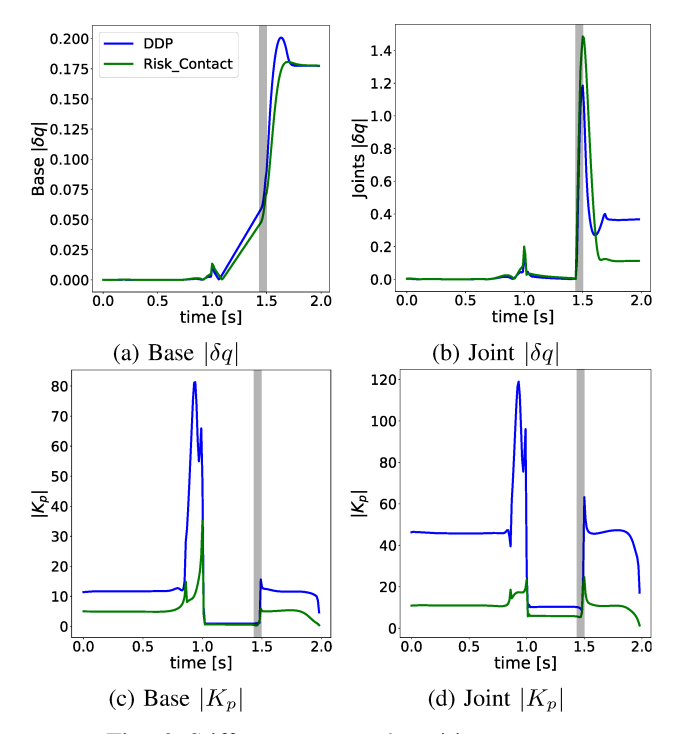


Fig. 6: Stiffness norm and position errors.

during the support phase, the stiffness to damping ratio of risk sensitive is 1.5 times higher than that of DDP, explaining the good tracking with lower overall gain profiles.

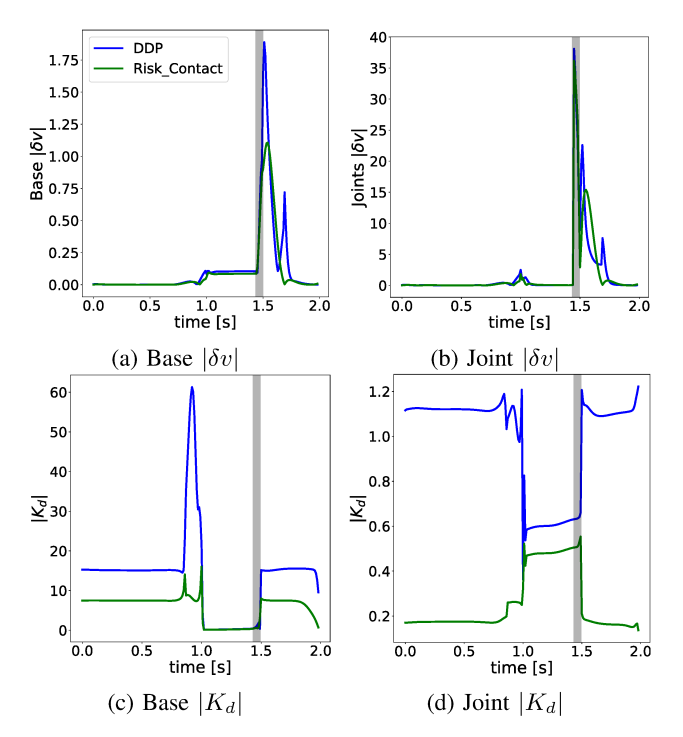


Fig. 7: Damping and Velocity Errors

C. Trade-off between Stability & Accuracy

In this experiment, we study the capabilities of our controller when trotting on unknown terrain. Both DDP and risk sensitive policies are optimized to track a trotting gait including a total of 14 contact switches. During simulations, we introduce unexpected blocks at contact locations (Fig. 10) in order to study the policies robustness. An execution is

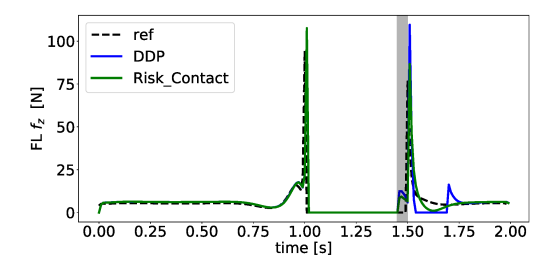
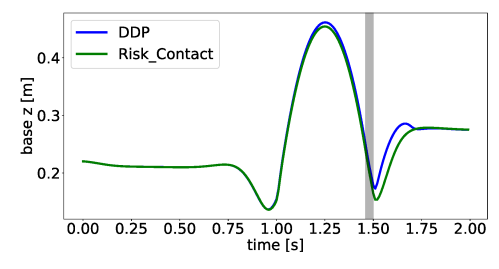
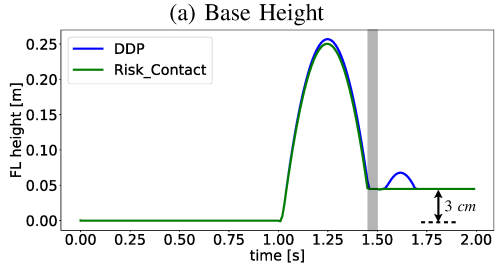


Fig. 8: FL Normal Contact Forces





(b) Front Left Foot Height

Fig. 9: Base and Foot Height Comparison

successful if the robot manages to reach the desired terminal base configuration and velocity without falling.

We conduct 1000 simulations, divided into two batches. In the first batch, the contact disturbances are sampled to represent up to 14% of the total leg length, which is quite aggressive. In the second batch, the maximum contact variation is 11% of the leg length. The results are summarized in Table I. In both cases, we observe a significant increase in trotting performance when using the risk sensitive controller. Moreover, the magnitude of the gains of the DDP controller are outside of the range of gains admissible on the real robot while the risk sensitive controller gains are not (based on our preliminary investigations on the real robot). This result demonstrates that the risk-sensitive controller effectively improves the robustness to contact uncertainties.

For successful executions, we show the distribution of base position tracking errors in Fig. 11. When successful, the risk sensitive control policy finishes the trotting gait with larger deviations in the base configuration to generate higher number of stable execution, underlying the trade-off between accurate tracking and robustness to contact uncertainty.

	Experiment 1		Experiment 2	
# of Simulations	500		500	
Maximum # of blocks	14		14	
Maximum block height	45 mm		34 mm	
% of leg length	14 %		11 %	
Method	DDP	Risk	DDP	Risk
# of Successful Sim.	237	325	358	458
% of Successful Sim.	47.4%	65%	72.6%	91.6%

TABLE I: Parameters and results of the trotting experiments



Fig. 10: Snapshots of the trotting gait and the contact disturbances.

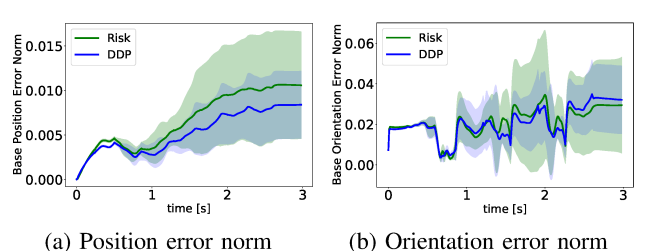


Fig. 11: Trotting Base Tracking Error Norms Statistics

V. CONCLUSION

In this paper, we extend the idea of risk sensitive optimal control with measurement uncertainty to legged locomotion problems. We show the importance of the choice of the noise models to generate meaningful impedance modulation patterns. Through extensive simulations, we demonstrate that our approach can generate stiffness and damping profiles that lead to better responses in face of hard impacts and contact uncertainty when compared to typical DDP algorithms. The computed gains are significantly smaller, and within ranges that are realistically executable on the real robot. Our approach provides a systematic approach to automatically compute optimal impedance modulations, at the same computational cost as modern DDP algorithms. Future work will include real robot experiments.

REFERENCES

- E. Burdet, R. Osu, D. W. Franklin, T. E. Milner, and M. Kawato, "The central nervous system stabilizes unstable dynamics by learning optimal impedance," *Nature*, vol. 414, no. 6862, pp. 446–449, 2001.
- [2] H. Lee, E. J. Rouse, and H. I. Krebs, "Summary of human ankle mechanical impedance during walking," *IEEE journal of translational* engineering in health and medicine, vol. 4, pp. 1–7, 2016.
- [3] D. Liu and E. Todorov, "Evidence for the flexible sensorimotor strategies predicted by optimal feedback control," *Journal of Neuroscience*, vol. 27, no. 35, pp. 9354–9368, 2007.
- [4] A. J. Nagengast, D. A. Braun, and D. M. Wolpert, "Risk-sensitivity and the mean-variance trade-off: decision making in sensorimotor control," *Proceedings of the Royal Society B: Biological Sciences*, vol. 278, no. 1716, pp. 2325–2332, 2011.
- [5] N. Hogan, "Impedance control-an approach to manipulation. i-theory. ii-implementation. iii-applications," ASME Journal of Dynamic Systems and Measurement Control B, vol. 107, pp. 1–24, 1985.
- [6] —, "Stable execution of contact tasks using impedance control," in 1987 IEEE International Conference on Robotics and Automation, vol. 4. IEEE, 1987, pp. 1047–1054.
- [7] J. H. Park, "Impedance control for biped robot locomotion," *IEEE Trans. on Robotics and Automation*, vol. 17, no. 6, pp. 870–882, 2001.
- [8] J. Lee, D. J. Hyun, J. Ahn, S. Kim, and N. Hogan, "On the dynamics of a quadruped robot model with impedance control: Self-stabilizing high speed trot-running and period-doubling bifurcations," in *IEEE/RSJ International Conference on Intelligent Robots and Systems*, 2014.
- [9] D. Mayne, "A second-order gradient method for determining optimal trajectories of non-linear discrete-time systems," *International Journal* of Control, vol. 3, no. 1, pp. 85–95, 1966.
- [10] W. Li and E. Todorov, "Iterative linear quadratic regulator design for nonlinear biological movement systems." in *ICINCO*, 2004.
- [11] A. Sideris and J. E. Bobrow, "An efficient sequential linear quadratic algorithm for solving nonlinear optimal control problems," in *American Control Conference*. IEEE, 2005, pp. 2275–2280.

- [12] Y. Tassa, T. Erez, and E. Todorov, "Synthesis and stabilization of complex behaviors through online trajectory optimization," in *IEEE/RSJ* International Conference on Intelligent Robots and Systems, 2012.
- [13] Y. Tassa, N. Mansard, and E. Todorov, "Control-limited differential dynamic programming," in 2014 IEEE International Conference on Robotics and Automation (ICRA). IEEE, 2014, pp. 1168–1175.
- [14] R. Grandia, F. Farshidian, A. Dosovitskiy, R. Ranftl, and M. Hutter, "Frequency-aware model predictive control," *IEEE Robotics and Automation Letters*, vol. 4, no. 2, pp. 1517–1524, 2019.
- [15] R. Grandia, F. Farshidian, R. Ranftl, and M. Hutter, "Feedback mpc for torque-controlled legged robots," in 2019 IEEE/RSJ International Conference on Intelligent Robots and Systems (IROS). IEEE, 2019, pp. 4730–4737.
- [16] E. Todorov and W. Li, "A generalized iterative lqg method for locally-optimal feedback control of constrained nonlinear stochastic systems," in *American Control Conference*, 2005, pp. 300–306.
- [17] W. Li and E. Todorov, "Iterative linearization methods for approximately optimal control and estimation of non-linear stochastic system," *International Journal of Control*, vol. 80, no. 9, pp. 1439–1453, 2007.
- [18] D. Jacobson, "Optimal stochastic linear systems with exponential performance criteria and their relation to deterministic differential games," *IEEE Tran on Aut. control*, vol. 18, no. 2, pp. 124–131, 1973.
- [19] F. Farshidian and J. Buchli, "Risk sensitive, nonlinear optimal control: Iterative linear exponential-quadratic optimal control with gaussian noise," arXiv preprint arXiv:1512.07173, 2015.
- [20] J. R. Medina and S. Hirche, "Considering uncertainty in optimal robot control through high-order cost statistics," *IEEE Transactions on Robotics*, vol. 34, no. 4, pp. 1068–1081, 2018.
- [21] B. Pontón, S. Schaal, and L. Righetti, "On the effects of measurement uncertainty in optimal control of contact interactions," in *Algorithmic Foundations of Robotics XII*. Springer, 2020, pp. 784–799.
- [22] G. Gilardi and I. Sharf, "Literature survey of contact dynamics modelling," *Mechanism and machine theory*, vol. 37, pp. 1213–1239, 2002.
- [23] L. Righetti, J. Buchli, M. Mistry, M. Kalakrishnan, and S. Schaal, "Optimal distribution of contact forces with inverse-dynamics control," *The International Journal of Robotics Research*, vol. 32, no. 3, pp. 280–298, 2013.
- [24] K. Dvijotham and E. Todorov, "A unifying framework for linearly solvable control," in *Proceedings of the Twenty-Seventh Conference on Uncertainty in Artificial Intelligence*, 2011, pp. 179–186.
- [25] C. Mastalli, R. Budhiraja, W. Merkt, G. Saurel, B. Hammoud, M. Naveau, J. Carpentier, L. Righetti, S. Vijayakumar, and N. Mansard, "Crocoddyl: An efficient and versatile framework for multi-contact optimal control," in 2020 IEEE International Conference on Robotics and Automation (ICRA). IEEE, 2020, pp. 2536–2542.
- [26] J. Speyer, J. Deyst, and D. Jacobson, "Optimization of stochastic linear systems with additive measurement and process noise using exponential performance criteria," *IEEE Transactions on Automatic Control*, vol. 19, no. 4, pp. 358–366, 1974.
- [27] V. Roulet, M. Fazel, S. Srinivasa, and Z. Harchaoui, "On the convergence of the iterative linear exponential quadratic gaussian algorithm to stationary points," in *IEEE American Control Conference*, 2020.
- [28] B. Ponton, A. Herzog, A. Del Prete, S. Schaal, and L. Righetti, "On time optimization of centroidal momentum dynamics," in *IEEE International Conference on Robotics and Automation*. IEEE, 2018.
- [29] J. Carpentier, G. Saurel, G. Buondonno, J. Mirabel, F. Lamiraux, O. Stasse, and N. Mansard, "The pinocchio c++ library: A fast and flexible implementation of rigid body dynamics algorithms and their analytical derivatives," in *IEEE/SICE International Symposium on Sys*tem Integration, 2019, pp. 614–619.
- [30] J. Sola, "Quaternion kinematics for the error-state kalman filter," arXiv preprint arXiv:1711.02508, 2017.
- [31] F. Grimminger, A. Meduri, M. Khadiv, J. Viereck, M. Wüthrich, M. Naveau, V. Berenz, S. Heim, F. Widmaier, T. Flayols *et al.*, "An open torque-controlled modular robot architecture for legged locomotion research," *IEEE Robotics and Automation Letters*, vol. 5, no. 2, pp. 3650–3657, 2020.
- [32] B. Hammoud, L. Olivieri, L. Righetti, J. Carpentier, and A. Del Prete, "Fast and accurate multi-body simulation with stiff viscoelastic contacts," arXiv preprint arXiv:2101.06846, 2021.